World Scientific
www.worldscientific.com

Biological Motion Aids Gestural Communication by Humanoid Social Robots

Adedayo Akinade ⓘ*, Daniel Barros ⓘ† and David Vernon ⓘ‡

Carnegie Mellon University Africa, Kigali, Rwanda
*aakinade@andrew.cmu.edu
†dbarros@andrew.cmu.edu
‡dvernon@andrew.cmu.edu

Advances in social robotics have led to increased interest in designing robots that can communicate effectively with humans through nonverbal gestures. One approach to enhancing the naturalness and expressiveness of robot gestures is to incorporate biological motion, which mimics the velocity and acceleration profiles observed in human gestures. This paper examines the use of biological motion for gestural communication by humanoid social robots, focusing on the impact of biological motion on the perceived warmth and effectiveness of robot gestures in fostering engagement while interacting with these robots. The exercise involved implementing the minimum jerk model of biological motion on a Pepper humanoid social robot and conducting user studies to evaluate the impact of biological motion on human–robot interaction. The results show that incorporating biological motion cues can significantly increase the perceived warmth of robot gestures and improve the overall effectiveness of gestural communication, resulting in more natural and engaging human–robot interaction.

Keywords: Human–robot interaction; social robotics; biological motion; minimum jerk; two-thirds power law.

1. Introduction

Social robots are designed to be autonomous or semi-autonomous machines that engage with people through social interactions, aiming to communicate in ways that adhere to human social and cultural norms.[1] One of the primary goals in developing these robots is to enhance user experience by enabling natural and intuitive communication. Ideally, social robots are envisioned to understand and respond to

human emotions, intentions, and social cues with a degree of social and emotional intelligence.[2] While many current systems demonstrate some level of social competency and the ability to maintain basic social bonds through imitation and interaction, the field aspires to further capabilities such as genuine individuality, social learning, and adaptive behavior that responds to the social environment and individual needs.[3,4] These characteristics, though central to the goals of social robotics, remain a blend of realized features and ongoing challenges in advancing human–robot social interaction.

Social robots can have a positive impact on society in fields like healthcare,[5] education,[6,7] and elderly care,[8] where they are being used to support and help people in a variety of contexts. For example, they are used in healthcare to provide patients company, emotional support, and medication reminders. They are also used in education as instructional aids to improve student engagement and learning experiences through interactive, individualized activities, helping to improve educational results and provide a suitable learning environment by offering personalized support and feedback.[9]

The field of human–robot interaction (HRI) focuses on modelling and implementing effective interaction between humans and robots, with robots comprehending needs of humans and reacting to social cues.[10] By leveraging insights from social cognition, psychology, and neuroscience, HRI research aims to improve human-robot interactions by making them more efficient, meaningful, and natural,[11] developing robots that can engage with humans in a human-like manner, establishing rapport, and fostering trust by exhibiting empathetic behavior.[12]

Nonverbal communication is a key aspect of such human interaction. This includes body language, gesture, and facial expression. These cues improve interpersonal communication by conveying an array of information.[13,14] Complementing linguistic communications, they provide social and emotional cues that can improve interpersonal communication.[15,16] Gestures and facial expressions can enhance verbal communication by expressing emotions, intentions, and emphasis.[13,14] Even though the significance of nonverbal communication in HRI is widely acknowledged, existing approaches to incorporating these skills in social robots frequently fail to capture the expressive and organic nature of human body language and gestures.

Biological motion has the potential for developing more expressive, natural, and socially engaging robotic motions by making the robots appear more natural and comfortable for humans to interact with.[17] The term describes the organic, realistic characteristics of human and animal movement, which is distinguished by fluidity, coordination, and expressiveness,[18] as opposed to the jerky and squared motion exhibited by robotic actions.[19] Complicated spatiotemporal patterns that control the movement of many body components are fundamental to biological motion. When it comes to the perception of naturalness and expressiveness in movements, human gestures and body language demonstrate complex coordination between the limbs, torso, and head with subtle changes in timing, velocity, and acceleration. Complex musculoskeletal mechanisms and neuromotor control systems that underpin human movement produce these biological motion patterns.[18] These characteristics may be

used to design and regulate the motions of social robots, allowing the creation of robotic gestures and behaviors that are more akin to the subtlety and fluidity of human nonverbal communication.[20] The coordinated limb motions, recognizable velocity profiles, and delicate anticipatory and transitional dynamics that characterize real human motion may all be replicated in this way.[21] While the goal of a movement plays a vital role in engaging interactions, the movement kinematics, e.g., the velocity profile might also vary the degree of motor resonance evoked in the interaction partner, which has been linked to humans' ability to engage in interactions with other partners, resulting in "mutual understanding".[19]

The goal of the research described in this paper is to enhance the social interaction capabilities of a humanoid robot through the implementation and evaluation of gestures which comprise movements that exhibit the characteristics of biological motion, thereby improving its naturalness and warmth as perceived by human partners in human-robot interactions.

2. Models of Biological Motion

There are two principal approaches to modelling biological motion: the two-thirds power law and the minimum jerk model. We discuss both approaches in the following.

2.1. *Two-thirds power law*

The two-thirds power law[22–26] has been shown to characterize many kinds of human movement, including locomotion[27] and ocular motion.[28] The perception[29,28,30] and anticipation[31] of human motion are also characterized by this law. The isogony principle, which states that people's movements generally span identical angles in equal amounts of time regardless of the true arc length of the spatial trajectory, shows a strong link between the velocity profile and curvature of human motion. The two-thirds power law formalizes this relationship, as follows:

$$V(t) = K(t)\left(\frac{R(t)}{1 + \alpha R(t)}\right)^{\beta},\tag{1}$$

where $V(t)$ is the tangential velocity at time t and $R(t)$ is the radius of curvature at that same instant.

The value of the β exponent, which has been empirically demonstrated to be in agreement with the value of $\frac{1}{3}$ over a large class of human motion, demonstrates the regularity of human motion.[24,32,22] The remaining two variables in the equation are $K(t) > 0$ and $\alpha \in [0, 1]$. When there are no points of inflection on the trajectory, $K(t)$ is zero; otherwise, it is determined by the motion's average velocity. The second variable α, sometimes referred to as the velocity gain factor, is influenced by the speed and duration of the motion.[23,33] Experiments have shown that only one value of K is insufficient to explain the data for longer or uncontrolled motions, even if its exact role is still unknown. It has been highlighted[24,34] how its value typically stays

constant for quite lengthy portions of the trajectories and tends to alter in accordance with junction points of inflection.

In the case where $\alpha = 0$, the law can be simplified as

$$V(t) = K(t)R(t)^{\beta}, \tag{2}$$

from which we can derive the alternative formulation

$$A(t) = K(t)C(t)^{1-\beta} = K(t)C(t)^{\frac{2}{3}}, \tag{3}$$

hence, the two-thirds power law formulation, where $A(t) = \frac{V(t)}{R(t)}$ is the angular velocity, while $C(t) = \frac{1}{R(t)}$ is the curvature.

2.2. *Minimum jerk model*

The two-thirds power law is predicated on two assumptions: (a) the motor control system has access to a spatial plan before the motion begins, and (b) many immediate and kinematics elements of the motion are explicitly limited by the geometrical characteristics of the true planned trajectory.[33] Therefore, the two-thirds power law does not explicitly address the question of trajectory development. Conversely, in certain motion planning approaches that deviate from the motor program convention, the constraints that are intended to match the general qualitative characteristics of the motor system result in a much more global setting, which causes an appropriate loss in the degrees of freedom. Specifically, a number of researchers[35–39] have examined the effects of assuming that point-to-point motion adheres to a global minimum-cost constraint.

Natural motion — and, more significantly, hand motion — tends to appear fluid and elegant unless there are certain, limiting conditions. Then, it is possible to hypothesize that this distinguishing trait relates to a design concept, meaning that the motor system plans end-point motions based on a requirement of maximal smoothness.[40] This requirement allows one to formulate a motor control policy. In order to do this, a cost function (CF) proportional to the mean square of jerk (the derivative of acceleration) is defined as follows:

$$\mathrm{CF} = \frac{1}{2} \int_{t_1}^{t_2} \left[\left(\frac{d^3x}{dt^3} \right)^2 + \left(\frac{d^3y}{dt^3} \right)^2 \right] dt. \tag{4}$$

If the associated parametric models of the motor control policy minimize the cost CF, the motion is "maximally smooth". It can be shown that this minimal requirement plus a suitable set of boundary conditions can be satisfied by a pair of parametric equations.

The minimum jerk model suggests that the motor control system uses this specific pair for creating a trajectory. This is an optimal control problem with interior point equality constraints,[33] which generates a closed-form analytical solution in the relevant case corresponding to the movement from an initial point $Q_1 = (x_1, y_1)$ to a final point $Q_3 = (x_3, y_3)$ via an intermediate position $Q_2 = (x_2, y_2)$. Fifth-order

polynomial functions of time are used to represent the motion's horizontal and vertical components

$$x(t) = \sum_{k=0}^{5} c_{kx} t^k + p_{1x}(t - t_2)^4 + p_{2x}(t - t_2)_+^5,$$

$$y(t) = \sum_{k=0}^{5} c_{ky} t^k + p_{1y}(t - t_2)^4 + p_{2y}(t - t_2)_+^5, \tag{5}$$

$$(t - t_2)_+ = \begin{cases} (t - t_2) & \text{if } t \ge 2, \\ 0 & \text{if } t < 2, \end{cases}$$

where t_2 is the transit time via the via-point. The following set of boundary conditions can be used to compute the coefficients $\{c_{kx}, c_{ky}; k = 0, 5\}$, p_{1x}, p_{2x}, p_{1y}, and p_{2y}: time, position, velocity, and acceleration at Q_1 and Q_3, and position and velocity (or simply position) at Q_2.

The resultant model is both time homogeneous and scalable, meaning that shifts in time scale have no effect on the trajectory and are expressed proportionally in the kinematic parameters. It is invariant with regard to rotations and translations of the locations Q_1, Q_2, and Q_3. It needs to be emphasized that the boundary and minimum criteria work together to define the travel time t_2 at the via-point. As a result, the model forecasts the movement's underlying temporal structure quantitatively. Specifically, by predicting how the relative duration $(t_2 - t_1)/(t_3 - t_1)$ of the first part of the movement (up to the via-point) varies as a function of the corresponding relative length of the trajectory $(s_2 - s_1)/(s_3 - s_1)$, one can test the ability of the model to simulate the phenomenon of local isochrony. These predictions were found to be in agreement with the experimental results.[35]

2.3. *Decoupled minimum jerk model*

The minimum jerk profile has some limitations, such as the lack of variability and adaptability to different situations and targets.[41] Huber *et al.*[42] proposed a novel trajectory generator for HRI, based on a variation of the minimum jerk profile, a decoupled minimum jerk model. The authors introduced a parameter that controls the curvature of the trajectory, allowing the robot to approach the target from different angles. The trajectory generator was evaluated in a simple handover task, using a humanoid robot arm and a human participant. The authors used a post-test questionnaire to measure the human's comfort and acceptance of the robot's motion, as well as their perception of the robot's human likeness and safety. The results showed that the novel trajectory generator was comparable to the traditional minimum jerk profile in terms of comfort, human likeness, and subjective safety while offering some advantages in the target approach. The authors concluded that their trajectory generator can be used to generate more expressive and adaptive motion for robots in HRI.

The decoupled minimum jerk model treats the XY and Z components of the three-dimensional (3D) trajectory separately and by doing this decouples the height component of the movement from the planar component. This leads to a more

human-like trajectory. The literature has shown that if we decouple the z-axis motion from the xy-plane motion by specifying two minimum jerk trajectories with different durations for the two components, we obtain a curved trajectory that more closely resembles human handover reaching motions as the ending portion of the trajectory is still straight. This decoupled minimum jerk trajectory is described by

$$
\begin{aligned}
r_z(t) &= \sum_{k=0}^{5} a_{kz} t^k, \\
r_{xy}(t) &= \sum_{k=0}^{5} a_{kxy} t^k,
\end{aligned}
\tag{6}
$$

where $r_z(t)$ is the trajectory in the z-direction, with duration t_z, and $r_{xy}(t)$ is the trajectory in the xy-plane, with duration t_{xy}. The coefficients a_{kz} and a_{kxy} are again determined by boundary conditions. The decoupled minimum jerk trajectory results in a curved path in 3D space, residing in a plane orthogonal to the xy-plane. The ratio between t_z and t_{xy} is determined through optimization.

3. Biological Motion Trajectory Generation

For each gesture, the trajectory planning generates a trajectory that starts and ends smoothly, with minimal acceleration and deceleration. The trajectory is designed to be continuous and differentiable, ensuring that the robot's movements are smooth and natural. For a particular trajectory $x_1(t)$ that starts at time t_i and ends at time t_f, the smoothness can be measured by calculating a jerk cost

$$
\int_{t=t_i}^{t_f} \dddot{x}_1(t)^2 dt.
\tag{7}
$$

Note that jerk cost is a scalar; the expression above assigns a number to the function $x_1(t)$. Hogan showed what function $x(t)$ most smoothly connects a starting point to a target in a given amount of time.[43] This function $x(t)$, among all possible functions, has the minimum jerk cost. The form of the minimum jerk movement trajectory is a fifth-order polynomial in time

$$
\theta(t) = a_0 + a_1 t + a_2 t^2 + a_3 t^3 + a_4 t^4 + a_5 t^5,
\tag{8}
$$

where $a_0, \ldots, a_5$ are constants.

The details of a specific movement depend on its boundary conditions. A sufficient set of boundary conditions consists of the position (θ), velocity ($\dot{\theta}$), and acceleration ($\ddot{\theta}$) at the start of the movement ($t = 0$) and at the finish ($t = d$). The movements to be modeled start and finish at rest; thus the chosen boundary conditions for this point-to-point movement are as follows:

$$
\begin{aligned}
\theta(0) &= p_s; \quad \dot{\theta}(0) = 0; \quad \ddot{\theta}(0) = 0; \\
\theta(d) &= p_f; \quad \dot{\theta}(d) = 0; \quad \ddot{\theta}(d) = 0,
\end{aligned}
\tag{9}
$$

where p_s is the start position, p_f is the final position of the trajectory, θ is the position, $\dot{\theta}$ is the velocity, and $\ddot{\theta}$ is the acceleration.

Solving for the constants $a_0, \ldots, a_5$ yields the following equation for the position (θ), velocity ($\dot{\theta}$), and acceleration ($\ddot{\theta}$):

$$
\begin{aligned}
\theta(t) &= p_s + k[10(t/d)^3 - 15(t/d)^4 + 6(t/d)^5] \\
\dot{\theta}(t) &= \frac{k}{d}\left[30(t/d)^2 - 60(t/d)^3 + 30(t/d)^4\right] \\
\ddot{\theta}(t) &= \frac{k}{d^2}\left[60(t/d) - 180(t/d)^2 + 120(t/d)^3\right] \\
0 &\leq t \leq d
\end{aligned}
\tag{10}
$$

where k is the movement amplitude given by $k = p_f - p_s$.

Equation (9) shows that the shape of the predicted movement trajectory does not change with the amplitude or duration of the movement. Changes in movement amplitude or duration merely serve to change the scale of the position and time axes, respectively. The following characteristics of the movement may be derived:

$$
\begin{aligned}
&\text{Maximum velocity} = 1.88a/d, \\
&\text{Maximum acceleration} = 5.77a/d^2.
\end{aligned}
\tag{11}
$$

It can be seen from Eq. (11) that if the movement duration remains constant, the peak absolute acceleration will scale with movement amplitude. Within the limits of experimental accuracy, the minimum jerk movement profile yields good qualitative and quantitative agreement with observed undisturbed movement profiles.

4. Gesture Execution and Control

Based on the expressions for joint angle position, joint angle velocity and joint angle acceleration in Eq. (9), a trajectory generation module computed desired joint angle trajectories based on the selected gesture and its parameters. These trajectories were subsequently transformed into joint-level commands through inverse kinematics and motion control, ensuring smooth execution by a Pepper robot. The architecture of the gesture control system is shown in Fig. 1.
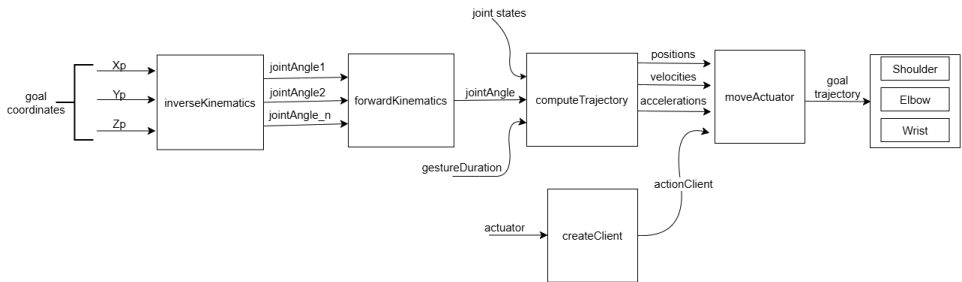

Fig. 1. Architecture of the gesture control system.

Given a goal coordinate x_p, y_p, z_p in 3D space representing a location is space to which the Pepper robot is to point, i.e., perform a deictic gesture, Algorithm 1 sets out the computational process whereby the deictic gesture is executed. The inverse kinematics are used to estimate the joint angles required to achieve this gesture. These joint angles are passed through the forward kinematics and the joint angle that produces the closest 3D position to the goal coordinates is selected. The trajectory is computed for the arm to move from the current joint states to the required joint angle, taking into consideration the required gesture duration. The trajectory information contains the positions, velocities and accelerations at the different points along the trajectory. This information is sent to the action server, along with the action client created for the actuator. The action server sends the required information to each of the joints of the actuator (shoulder, elbow, and wrist).

Throughout the execution and control process, safety and robustness were prioritized. It was ensured that the limits to the joint angles defined by the manufacturer for all joints were taken into consideration.

Algorithm 1. Gesture Execution Algorithm.

Require: $biologicalMotionFlag, actuatorJoint, gestureDuration, x_p, y_p, z_p$
Ensure: $gestureDuration > 0$
  $x \leftarrow x_p$
  $y \leftarrow y_p$
  $z \leftarrow z_p$
  $jointAngles \leftarrow$ inverseKinematics(x, y, z) ▷ Compute the joint angles
  for $jointAngle$ in $jointAngles$ **do**
      $x_f, y_f, z_f =$ forwardKinematics$(jointAngle)$ ▷ Obtain the position
      if $x_f, y_f, z_f = x, y, z$ **then** ▷ JointAngle is valid
          break
      else
          $status \leftarrow 0$
          return $status$
      end if
  end for
  $jointClient \leftarrow$ createClient$(actuatorJoint)$ ▷ Create ROS actionClient
  if $biologicalMotionFlag$ is True **then**
      $Positions, Velocities, Accelerations \leftarrow$ computeTrajectory$(jointAngle)$
      $status \leftarrow$ moveActuator$(jointClient, Positions, Velocities, Accelerations)$
  else
      $status \leftarrow$ moveActuator$(jointClient, jointAngle)$ ▷ Move the joint
  end if
  return $status$

---

5. Algorithm Implementation

The implementation of the decoupled minimum jerk model involves several key steps, including trajectory planning, motion control, and integration with the Pepper robot's software framework. The algorithms and techniques used to implement biological motion are discussed in this section.

Each gesture is defined by a set of key points that specify the desired position and orientation of the robot's end effector (e.g., hand or head) at specific times. The minimum jerk model is then used to interpolate between these key points, generating a smooth trajectory that the robot follows to perform the gesture.

To incorporate the minimum jerk model into the Pepper robot's software framework, a trajectory planning module that takes as input the key points for each gesture and generates the corresponding trajectories, was developed. These trajectories are then executed by the robot's motion control system, which ensures that the robot follows the planned trajectory accurately and smoothly. By using the minimum jerk model, the gestures executed are not only smooth and natural but also highly customizable. The model allows for the control of various aspects of the gesture, such as speed, acceleration, and curvature, providing fine-grained control over the robot's movements.

The implementation of the biological motion for gesture execution on the Pepper robot is realized as a Robot Operating System (ROS) node that provides a ROS service which listens for requests to the gesture service and executes the requested gesture based on the parameters provided. To interact with the gesture service, a client node sends requests to the service with the required gesture parameters, as follows.

- Gesture Type: The type of gesture to be executed (i.e., deictic, iconic, symbolic, bow, or nod).
- Duration: The duration of the gesture, controlling the speed at which the gesture is performed.
- Bow or Nod Angle: The torso angle at which the robot should bow or the head angle at which the robot should nod.
- Target Coordinate: The target coordinate in the world that the robot should point to, if the gesture is a deictic pointing gesture.

The client nodes are other elements of a complete system architecture for executing social robot missions.[44] The gestureExecution ROS node processes service requests from the behaviorController ROS node and subscribes to a ROS topic published by the robotLocalization ROS node to allow deictic gestures to be performed relative to the Pepper robot's current position and orientation. The gestureExecution ROS node can also send service requests to the overtAttention ROS node to direct the robot's gaze toward the location to which a deictic gesture points.

6. Integration with Pepper Robot

The integration of the gesture execution module with the Pepper robot's existing software framework is crucial for ensuring seamless communication and coordination between different components of the system. ROS actions provide a sophisticated mechanism for handling time-extended, preemptable tasks in robotic systems. Built upon the foundation of ROS topics and services, actions offer a flexible interface for executing complex behaviors that may require ongoing monitoring and potential cancellation. The action framework in ROS is structured around a client–server model. The action client, typically a high-level control node, sends goal requests to the action server, which is responsible for executing the task. This model facilitates the implementation of long-running operations while maintaining system responsiveness.

ROS actions coordinate complex behaviors that require feedback and goal completion. For example, the execution of a pointing gesture may require the robot to reach a specific target coordinate in the world. A ROS action server is used to handle this behavior, allowing the robot to move its arm and hand in a coordinated manner to point toward the target. The gesture execution module controls the robot's actuators, such as motors and joints, to execute the planned trajectories.

The gesture execution ROS node, gestureExecution, exploits a two-tiered approach to robot control, combining the ROS service for high-level command processing, i.e., gesture invocation by client node (specifically, the behaviorController ROS node in the system architecture[44]), with ROS actions for low-level joint actuation. This approach provides a flexible and efficient method for controlling the robot's movements. The hosted service acts as an interface layer, accepting control commands from the clients. When invoked, this service processes the incoming requests, translating them into appropriate commands for the robot. This abstraction layer allows for easy integration with various client applications and provides a standardized entry point for robot control. Upon receiving a control command, the hosted service initiates the appropriate ROS action to actuate the robot's joints. This relationship can be described as follows:

(1) Command Reception: The hosted service receives a request from a client.
(2) Command Processing: The service interprets the command and determines the required joint movements.
(3) Action Initiation: The service then triggers the corresponding ROS action, sending a goal that specifies the desired joint positions or movements.
(4) Joint Actuation: The ROS action server, responsible for direct communication with the robot's hardware, executes the goal by actuating the joints.
(5) Feedback and Monitoring: Throughout the execution, the ROS action provides feedback to the service, allowing for real-time monitoring of the task's progress.
(6) Result Reporting: Upon completion, the ROS action returns the result to the service, which can then relay the outcome back to the client.

This architecture leverages the strengths of both components: the hosted service provides a high-level, easily accessible interface for control, while the ROS action system handles the complexities of real-time joint actuation and monitoring. By using ROS actions for the actual joint control, we benefit from their preemptable nature and detailed feedback mechanisms, ensuring responsive and adaptable robot behavior. Moreover, this separation of concerns enhances the system's modularity. The hosted service can be updated or replaced without altering the underlying ROS action implementation, and vice versa, facilitating easier maintenance and future upgrades of the control system.

7. Experimental Design

The experimental design consisted of three interconnected experiments aimed at evaluating the execution and perception of motion profiles in the Pepper humanoid robot. The first experiment focused on verifying the robot's adherence to the intended motion profiles, biological and trapezoidal, by analyzing joint state data, including generated commands and measured positions and velocities, for the robot's right arm. The second experiment investigated the robot's wrist motion during gesture execution using a RealSense RGB-D camera, analyzing the spatial trajectory and velocity in 3D space to assess the smoothness and consistency of the two motion profiles. The third experiment explored human perception of the robot's gestures through user studies, evaluating subjective responses across warmth and discomfort dimensions using the Robotic Social Attributes Scale (RoSAS).[45] Together, these experiments provided a holistic understanding of the robot's physical motion accuracy, trajectory characteristics, and their impact on human perception.

In all three experiments, there are two conditions, as follows.

Condition 1: Nonbiological (Control) Gestures. In the control condition, participants observed the Pepper robot performing a set of gestures generated without the incorporation of biological motion principles. These gestures were executed using a trapezoidal motion profile, which lacked the natural fluidity and expressiveness of the biological motion profile.

Condition 2: Biological Motion Profile. In this condition, participants observed the Pepper robot performing a similar set of gestures using the biological motion model implemented in this research. These gestures included deictic (pointing) gestures, as well as body gestures such as bowing and nodding.

7.1. *Verification of motion profile execution through joint state analysis*

The first experiment aimed to evaluate the execution of the motion profiles — biological motion and trapezoidal motion — on the Pepper humanoid robot by analyzing the generated commands and the measured joint states. The primary

objective was to verify whether the robot accurately carried out the intended motion profiles and to assess the differences between the execution of these profiles. The experiment was conducted using the right arm of the Pepper robot, under the assumption that the arms of the robot are symmetric. It is therefore expected that the results observed for the right arm would also hold for the left arm, eliminating the need for duplicate experimentation on both arms.

The Pepper robot was programmed to execute a pre-defined deictic gesture with its right arm, specifically using four joints: shoulder roll, shoulder pitch, elbow yaw, and elbow roll. Commands were generated for both motion profiles, and the following data were recorded:

(1) Generated Commands: The trajectory positions and velocities defined for both motion profiles.
(2) Measured Joint States: The actual trajectory positions and velocities as executed by the robot, recorded from its joint sensors.

To account for potential measurement noise in the robot's sensors, the trajectory position data from the measured joint states were denoised using a Gaussian filter with a sigma value of 3. This step ensured smoother data for more accurate comparison against the generated commands. Since the trapezoidal motion profile lacks explicit velocity constraints, velocity commands were only generated for the biological motion profile. However, to evaluate velocity performance for both motion profiles, the measured joint velocities were computed using a finite-difference gradient method with a stencil size of 3. This approach enabled a consistent comparison between the velocity characteristics of the two profiles.

The recorded data were analyzed to assess the robot's ability to execute the specified motion profiles in two ways, as follows:

(1) Comparison of Trajectory Positions: The generated and measured positions for each joint were compared to verify adherence to the respective motion profiles.
(2) Comparison of Velocity Profiles: The velocity commands for the biological motion profile were compared against the computed velocities from the measured joint states. Additionally, the velocity profile of the measured joint states was analyzed to assess differences between trapezoidal and biological motion profiles.

7.2. *Trajectory and velocity analysis of wrist motion during gesture execution*

In the second experiment, the motion of the Pepper robot's wrist was analyzed during gesture execution using two distinct motion profiles: biological and trapezoidal. An ArUco marker was attached to the robot's wrist, and an Intel RealSense RGB-D camera was used to track its motion. The camera was positioned horizontally at a distance of 1.1 m from the robot, ensuring a clear view of the robot's

movements. The trajectory of the wrist was recorded in 3D space, capturing its positions along the x-, y-, and z-axes during the gestures.

To evaluate the velocity profile of the wrist motion, the recorded positional data were processed using a finite-difference gradient with a stencil size of 3. This allowed for accurate computation of the velocity trajectories for each axis. The experiment aimed to compare the trajectory and velocity profiles of the wrist between the biological and trapezoidal motion profiles, providing insights into the kinematic differences and smoothness of the two motion execution methods.

To ensure robustness, the trajectories were captured over 10 repeated trials for each motion profile. Velocity profiles of the wrist were also computed by taking the finite-difference gradient of the positional data, with a stencil size of 3 to enhance accuracy. Furthermore, statistical metrics, including the mean and standard deviation of the trajectory and velocity profiles, were calculated for each axis (x, y, and z) to quantify the variability in motion.

The analysis was conducted to compare the biological and trapezoidal motion profiles, focusing on differences in smoothness, consistency, and adherence to the intended trajectories. These data provided insights into the kinematic characteristics of the robot's wrist motion, contributing to a deeper understanding of the physical differences between the two motion profiles.

7.3. *Evaluation of user perception*

The third experiment aimed to evaluate the impact of biologically inspired motion on the perceived social attributes of the Pepper humanoid robot. This was achieved through a controlled user study where participants observed the robot executing gestures using two distinct motion profiles: biological and nonbiological (trapezoidal). The evaluation employed the RoSAS, a well-established tool in social robotics research, to assess dimensions of warmth and discomfort, which are critical for understanding HRI dynamics.[45–48]

In this study, 17 participants (seven females and 10 males), who were graduate students at the Carnegie Mellon University Africa in Rwanda, were recruited and exposed to a within-subjects experimental design. Each participant observed the Pepper robot perform a deictic gesture executed under two conditions: (1) a trapezoidal motion profile, which lacked the smoothness and natural characteristics of biological motion, and (2) a biological motion profile, which utilized the minimum jerk model to mimic natural human movement. Figure 2 shows the Pepper robot performing a gesture during the experiment. The study followed a within-subjects design, where each participant was exposed to two experimental conditions, without prior knowledge of what the gestures executed in each conditions entailed. It is important to note that nine of the participants had no prior experience working with humanoid robots, while the other eight had some experience.

The order of the conditions was randomly assigned to participants to mitigate potential-order effects. Participants were randomly assigned to either observe the

Fig. 2. The Pepper robot performing a deictic pointing gesture during the experiment. Note that the robot's gaze is directed to the object to which it is gesturing. The picture is taken from the perspective of the user in the study.

gestures executed using biological motion first, followed by the control gestures, or vice versa. As a result, 10 of the participants observed the trapezoidal motion profile first, while the other seven participants observed the biological motion profile first.

After observing the robot's gestures in each condition, participants were asked to complete a survey based on RoSAS. The survey instrument consisted of 19 questions, with 11 questions evaluating the warmth dimension and eight questions assessing the discomfort dimension. The warmth dimension encompassed attributes like naturalness, fluidity, expressiveness, and friendliness, while discomfort captured impressions such as awkwardness, uneasiness, and unnaturalness. Participants rated their perceptions using a seven-point Likert scale (1 = strongly disagree, 7 = strongly agree).

This experimental design enabled a direct comparison of human perception of the robot's gestures under both motion profiles. By analyzing participants' responses, the study sought to determine whether biologically inspired motion enhanced the perceived warmth of the robot and reduced discomfort, thereby advancing our

understanding of how motion profiles influence social perceptions of humanoid robots. The evaluation framework builds on previous applications of RoSAS in social robotics, which have demonstrated its utility in measuring social traits like anthropomorphism, competence, and engagement across diverse contexts and cultural settings.[49,50]

8. Results

This section presents the outcomes of three interrelated experiments conducted to evaluate the effectiveness of the biologically inspired motion model relative to the conventional trapezoidal motion model. Together, these experiments provide a complementary assessment of the proposed approach, integrating both objective performance metrics and subjective user evaluations.

The first experiment entailed a quantitative analysis of joint behavior, wherein the robot's generated and measured commands were compared in terms of joint positions and velocities. This analysis was aimed at evaluating the fidelity of joint execution and the robot's ability to adhere to planned motion trajectories, thus providing insight into the robustness of the control system under each motion profile.

The second experiment involved a detailed motion analysis of the robot's end-effector, focusing on the trajectory and velocity of the wrist during gesture execution. This experiment sought to quantify differences in motion smoothness, continuity, and naturalness between the biologically inspired and trapezoidal trajectories, thereby shedding light on the biomechanical implications of the proposed model. To assess repeatability, we present the mean, standard error, and variance for the trajectory across multiple repetitions.

The third experiment consisted of a user study designed to evaluate human perceptions of the robot's gestures under both motion profiles. Using the RoSAS, participants assessed the robot's warmth and discomfort dimensions. This subjective evaluation complements the objective data by examining how the differences in motion profiles influence the perceived social attributes of the robot.

This section integrates findings from joint behavior analysis, motion trajectory evaluation, and user studies to provide a holistic assessment of the proposed biologically inspired motion model. The results are organized into subsections that detail the methodology, statistical analysis, and key findings of each experiment, highlighting the significant differences between the motion profiles.

### 8.1. *Robot joint performance during gesture execution*

This experiment aimed to evaluate the alignment between the robot's generated joint commands and its measured joint behavior during gesture execution under both biological and trapezoidal motion profiles. The analysis (shown in Fig. 3) focused on four key joints of the Pepper robot: shoulder roll, shoulder pitch, elbow yaw, and elbow roll. The comparison considered the positions and velocities of each joint,
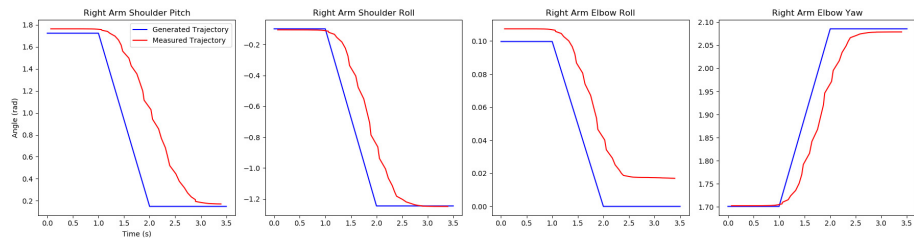
(a) Proprioceptive position plots demonstrating the Pepper robot's controller tracking the trapezoidal motion trajectory (blue). Measured positions (red) are denoised using a Gaussian filter ($\sigma = 3$)
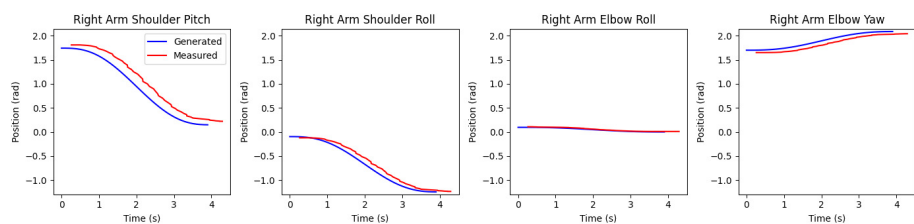
(b) Proprioceptive position plots demonstrating the Pepper robot's controller tracking the biological motion trajectory (blue). Measured positions (red) are denoised using a Gaussian filter ($\sigma = 3$)
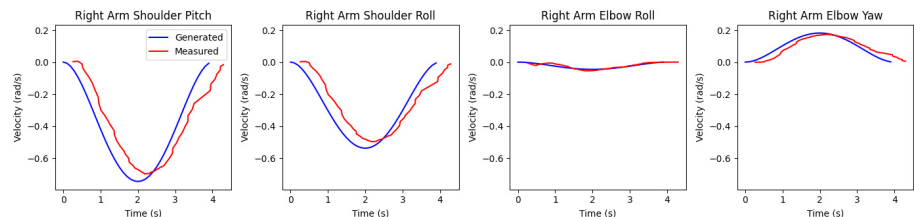
(c) Proprioceptive velocity plots demonstrating the Pepper robot's controller tracking the trapezoidal motion trajectory (blue). Measured velocities (red) are computed using a finite-difference gradient with a stencil of 3.
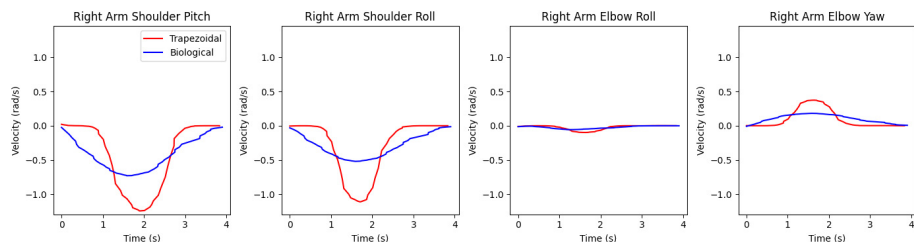
(d) Comparison of velocities derived from measured positions during control with trapezoidal (red) and biological (blue) motion. Velocity computation uses a finite-difference gradient with a stencil of 3.

Fig. 3.   (Color online) Comparison of generated and measured commands for four robot joints (shoulder roll, shoulder pitch, elbow yaw, elbow roll) during gesture execution. (a) Joint positions for the biological motion profile, (b) joint velocities for the biological motion profile, (c) joint positions for the trapezoidal motion profile, and (d) comparison of joint velocities between biological and trapezoidal motion profile.

providing insights into the robot's ability to execute commands with high fidelity across different motion profiles.

Figure 3(a) provides a comparison of the generated and measured joint positions during the execution of gestures with the trapezoidal motion profile. While the overall alignment is satisfactory, the trapezoidal motion profile exhibits sharper transitions in joint positions, leading to noticeable discrepancies between the generated and measured values. These sharp transitions are inherent to the profile's kinematic characteristics and contribute to less fluid motion compared to the biological profile.

Figure 3(b) illustrates the comparison between the generated and measured joint positions for each of the four robot joints during the execution of gestures with the biological motion profile. The data reveal a close alignment between the generated and measured values, indicating the robot's ability to effectively replicate the desired joint trajectories. Minor deviations observed in the measured positions can be attributed to hardware limitations and dynamic interactions during execution.

Figure 3(c) shows the comparison between the generated and measured joint velocities for the biological motion profile. The velocity data demonstrate consistent performance across all joints, with the measured velocities closely following the generated commands. Notably, the biological motion profile resulted in smooth velocity transitions, reflecting its effectiveness in mimicking human-like movement. Deviations in the measured velocities, while minimal, highlight the challenges in achieving perfect dynamic accuracy under varying operational conditions.

Figure 3(d) presents a direct comparison of the measured joint velocities for the biological and trapezoidal motion profiles. The biological profile demonstrates smoother velocity curves with gradual accelerations and decelerations, in contrast to the trapezoidal profile, which shows abrupt changes at transition points. These findings support the hypothesis that the biological profile produces more fluid and natural motion, while the trapezoidal profile introduces mechanical rigidity.
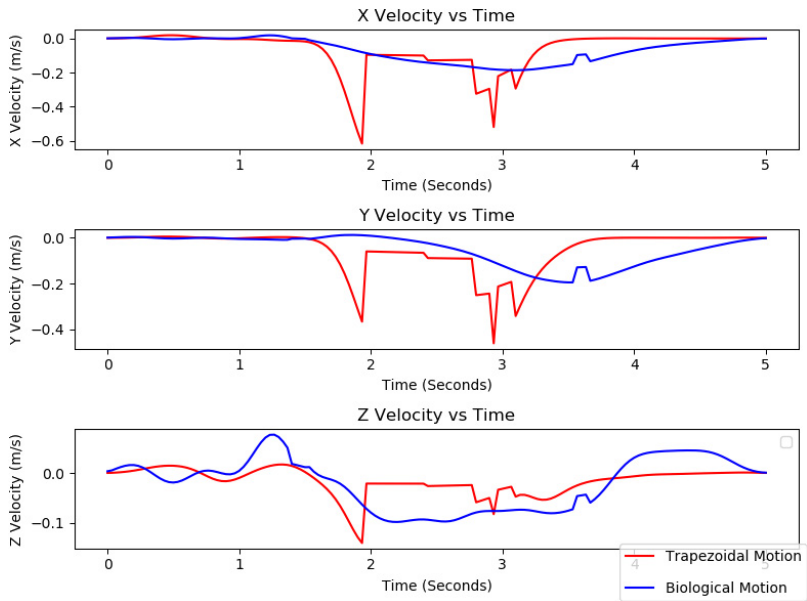
8.2. *Motion analysis of robot wrist trajectory*

This experiment aimed to analyze the trajectory of an ArUco marker, which was placed on the Pepper robot's wrist during gesture execution. Using a RealSense RGB-D camera, the Cartesian (x, y, z) coordinates of the robot wrist were tracked as the gestures were executed with both the biological and trapezoidal motion profiles. The analysis (shown in Figs. 4 and 5) focused on comparing the positions and velocities of the wrist trajectory under the two motion profiles, along with an evaluation of their variability across multiple runs.

Figure 4(a) illustrates the trajectory positions of the robot's wrist in the (x, y, z) coordinates during gesture execution. The comparison between the biological and trapezoidal motion profiles highlights distinct differences in trajectory smoothness. The biological motion profile generates smoother and more continuous wrist trajectories, closely following the desired path, whereas the trapezoidal motion profile exhibits sharper transitions and deviations at key points along the trajectory.
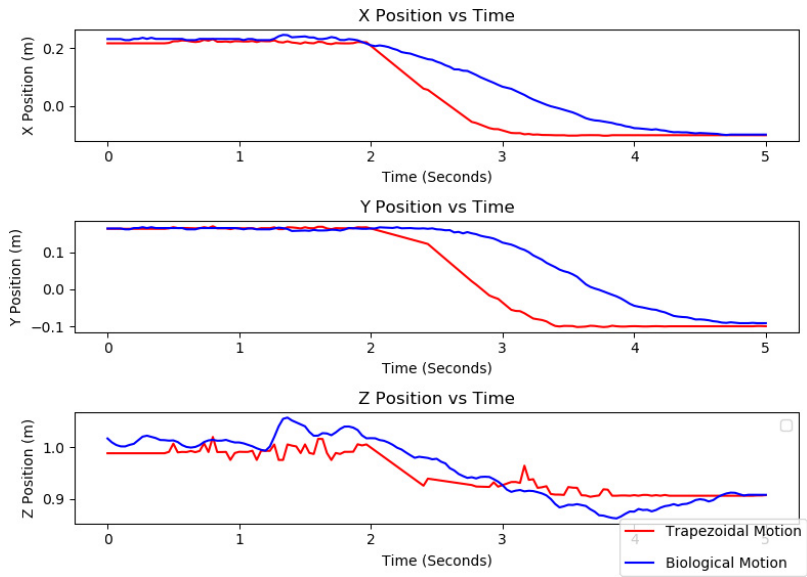
(a) Comparison of wrist trajectory positions (x, y, z) between the trapezoidal and biological motion profiles.

(b) Comparison of wrist trajectory velocities (x, y, z) between the trapezoidal and biological motion profiles.

Fig. 4. Analysis of wrist trajectory positions and velocities in the (x, y, z) coordinates during gesture execution for biological and trapezoidal motion profiles. (a) Wrist trajectory positions for biological and trapezoidal motion profiles, (b) wrist trajectory velocities for biological and trapezoidal motion profiles.

Figure 4(b) presents the wrist trajectory velocities for the (x, y, z) coordinates under both motion profiles. The biological motion profile demonstrates gradual changes in velocity, indicative of its human-inspired design. In contrast, the trapezoidal motion profile shows abrupt velocity transitions at points where acceleration and deceleration occur, resulting in less fluid motion. These findings reinforce the hypothesis that the biological motion profile is better suited for applications requiring natural and human-like movements.

Figure 5(a) depicts the mean and standard deviation of the wrist trajectory positions in the (x, y, z) coordinates over 10 independent runs for both motion profiles. The biological motion profile exhibits lower variability across runs, suggesting higher consistency and reproducibility in trajectory execution. In contrast, the trapezoidal motion profile demonstrates larger standard deviations, indicating higher sensitivity to dynamic and environmental factors during execution.

Figure 5(b) shows the mean and standard deviation of the wrist trajectory velocities in the (x, y, z) coordinates over 10 independent runs. Similar to the position analysis, the biological motion profile results in lower velocity variability, supporting its effectiveness in delivering consistent and predictable motion. The trapezoidal profile, however, shows larger variability, which may impact the perceived reliability and predictability of the robot's gestures.

8.3. *User response evaluation*

This section presents an analysis of the survey data collected to evaluate the impact of biologically inspired gestures on the perceived social attributes of the Pepper robot, focusing on the warmth and discomfort dimensions as measured by the RoSAS. We begin by outlining the statistically significant differences observed between the two gesture profiles (biological and trapezoidal), specifying the significance levels for each comparison. Box plots were generated to illustrate the mean and standard deviation of user responses, offering insights into the relative impact of motion profiles on perceived robot attributes. The overall comparison of the means obtained from the two conditions in both the warmth and discomfort is shown in Fig. 6. This figure provides a general view of user preferences relative to the neutral point[a] on the scale, highlighting differences between the motion profiles. The biological motion profile (represented in shades of green) demonstrates higher ratings above the midpoint for warmth and lower ratings below the midpoint for discomfort compared to the trapezoidal motion profile (represented in shades of red).

8.3.1. *Warmth dimension analysis*

The overall warmth dimension for the two experiments was analyzed based on four aspects: *naturalness*, *fluidity of motion*, *expressiveness of gestures*, and *perceived friendliness of the robot*.

---

[a] The neutral point is 4.0 on the scale.
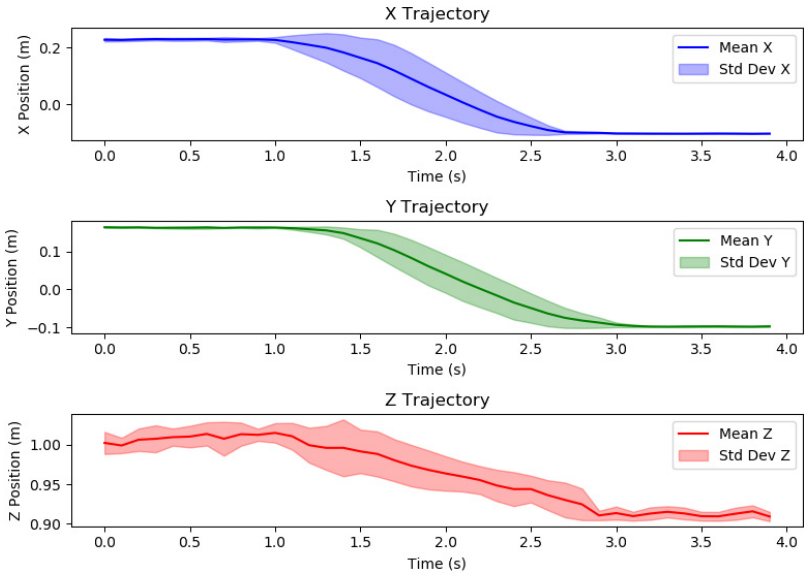
(a) Mean and standard deviation of wrist trajectory positions (x, y, z) across 10 runs for the biological motion profile.
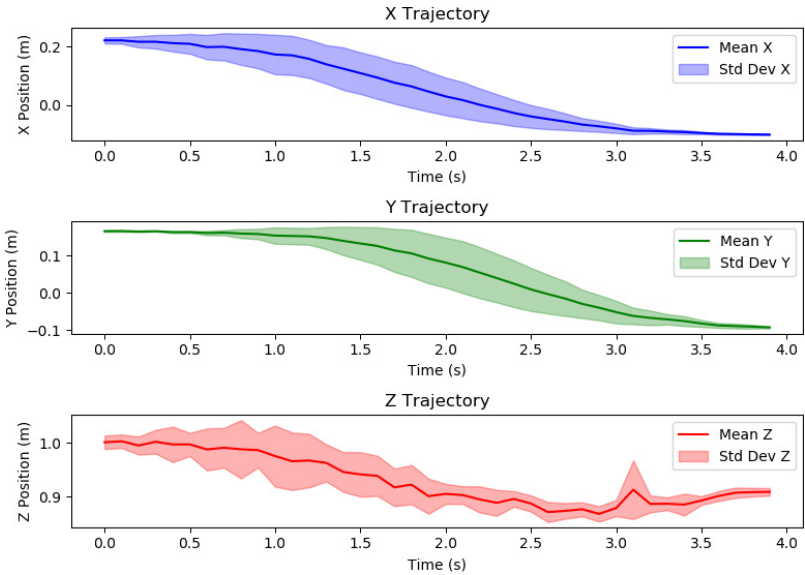
(b) Mean and standard deviation of wrist trajectory velocities (x, y, z) across 10 runs for both trapezoidal and biological motion profile.

Fig. 5. Analysis of wrist trajectory positions and velocities across multiple repetitions in the (x, y, z) coordinates during gesture execution for biological and trapezoidal motion profiles. (a) Mean and standard deviation of trajectory positions across 10 runs, and (b) Mean and standard deviation of trajectory velocities across 10 runs.
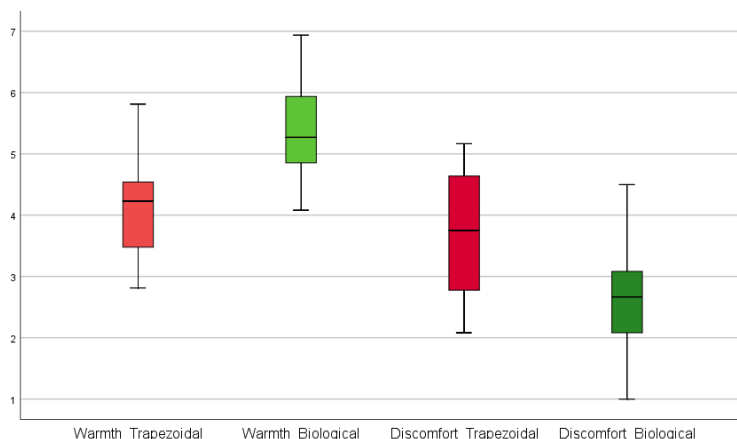
Fig. 6.   Mean of responses in the warmth and discomfort dimensions of Condition 1 (nonbiological control gesture) and Condition 2 (biological motion profile).

The results for the warmth dimension under the trapezoidal velocity profile revealed a mean score of 4.14 (SD[b]= 0.86, SE[c]= 0.21). The analysis showed no statistically significant difference from the midpoint ($t(16) = 0.664$, $p = 0.516$), with a mean difference of 0.14 and a 95% confidence interval ranging from -0.30 to 0.58. These findings suggest that the trapezoidal profile elicited a moderate perception of warmth, but the result was not significantly higher than the neutral point. In contrast, the biological motion profile achieved a higher mean score of 5.38 (SD = 0.83, SE = 0.20). The difference from the midpoint was statistically significant ($t(16) = 6.89$, $p < 0.001$), with a mean difference of 1.38 and a 95% confidence interval ranging from 0.96 to 1.80. These findings indicate that participants rated the biological motion profile as significantly above the neutral point on the warmth dimension.

The mean of the aspects of the warmth dimension under both conditions is shown in Fig. 7. This figure highlights how the biological motion profile (in shades of green) consistently scored higher across all sub-dimensions than the trapezoidal motion profile (in shades of red), indicating smoother and more human-like motion execution.

Naturalness: For the trapezoidal velocity profile, the naturalness score was relatively low, with a mean of 3.06 (SD = 1.16, SE = 0.28). The analysis revealed a significant difference from the midpoint ($t(16) = -3.35$, $p = 0.004$), with a mean difference of -0.94 and a 95% confidence interval of -1.54 to -0.35. These results suggest that the trapezoidal motion profile was perceived as significantly less natural than the neutral point. In comparison, the biological motion profile scored substantially higher, with a mean of 5.03 (SD = 1.33, SE = 0.32). The analysis showed a

[b] SD: standard deviation.
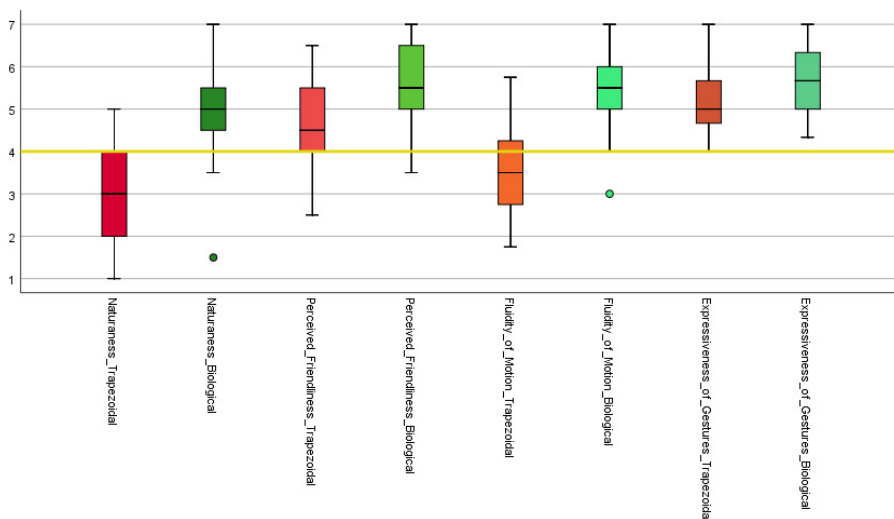[c] SE: standard error.

Fig. 7. Mean of responses of different aspects in the warmth dimension of Condition 1 (nonbiological control gesture) and Condition 2 (biological motion profile).

significant difference from the midpoint ($t(16) = 3.20$, $p = 0.006$), with a mean difference of 1.03 and a 95% confidence interval of 0.35–1.71. These findings indicate that the biological motion profile was perceived as significantly more natural than the neutral point. These results demonstrate that the biological motion profile aligns more closely with participants' expectations of naturalness, as indicated by its positive deviation from the neutral midpoint. This finding reinforces the idea that biologically inspired motion enhances the perceived realism and smoothness of robot gestures.

Fluidity of Motion: The trapezoidal motion profile resulted in a mean score of 3.51 (SD = 1.18, SE = 0.29). The analysis showed no statistically significant difference from the midpoint ($t(16) = -1.69$, $p = 0.11$), with a mean difference of -0.49 and a 95% confidence interval spanning from -1.09 to 0.12. These findings suggest that the trapezoidal motion profile did not strongly convey fluidity. These findings suggest that the trapezoidal motion profile did not strongly convey fluidity relative to a neutral perception. In contrast, the biological motion profile achieved a significantly higher mean score of 5.38 (SD = 1.04, SE = 0.25). The analysis revealed a significant difference from the midpoint ($t(16) = 5.51$, $p < 0.001$), with a mean difference of 1.38 and a 95% confidence interval of 0.85–1.91. These results indicate that the biological motion profile effectively conveyed a sense of fluidity, exceeding the neutral point by a meaningful margin. The biological motion profile was rated significantly higher in fluidity compared to the trapezoidal profile. This result underscores the importance of fluid motion in achieving natural and smooth gestures.

Expressiveness of Gestures: The trapezoidal velocity profile scored a mean of 5.27 (SD = 0.77, SE = 0.19). The analysis revealed a significant deviation from the midpoint ($t(16) = 6.86$, $p < 0.001$), with a mean difference of 1.27 and a 95% confidence interval of 0.88–1.67. These findings indicate that the trapezoidal motion profile conveyed a high level of expressiveness relative to a neutral perception. Similarly, the biological motion profile achieved an even higher mean score of 5.61 (SD = 0.81, SE = 0.20). The analysis showed a significant difference from the midpoint ($t(16) = 8.19$, $p < 0.001$), with a mean difference of 1.61 and a 95% confidence interval of 1.19–2.02. This demonstrates that the biological profile was also highly expressive, significantly exceeding the neutral point. Both motion profiles were rated as highly expressive when compared to the neutral midpoint. These findings suggest that both profiles are effective in conveying expressiveness in robot gestures, with the biological motion profile showing a slightly higher perceived expressiveness. This result suggests that incorporating biological motion profiles may not essentially influence the magnitude of expressiveness shown by the robot while executing the gestures.

Perceived Friendliness of Robot: For the trapezoidal motion profile, the mean score for perceived friendliness was 4.12 (SD = 0.79, SE = 0.19). The analysis revealed no significant difference from the midpoint ($t(16) = 0.643$, $p = 0.529$), with a mean difference of 0.12 and a 95% confidence interval of -0.29 to 0.53. These results indicate a neutral perception of friendliness for the trapezoidal profile. The biological motion profile achieved a higher mean score of 5.48 (SD = 0.84, SE = 0.20). The analysis showed a significant difference from the midpoint ($t(16) = 7.16$, $p < 0.001$), with a mean difference of 1.48 and a 95% confidence interval of 1.04–1.91. These results suggest that the biological profile significantly enhanced the perception of friendliness compared to the neutral midpoint. Both profiles were evaluated relative to the midpoint, with the trapezoidal profile eliciting a neutral response and the biological motion profile showing a significant positive perception of friendliness.

Paired *t*-test: In order to understand the actual difference between the warmth dimensions in the two conditions, a paired *t*-test was conducted between the overall warmth dimension for the linear and biological motion profiles. The results below showed a statistically significant difference ($t = -4.17, p = 0.001$), indicating that the biological motion profile was perceived as significantly warmer than the linear velocity profile.

These results provide insights into how participants perceived the robot's gestures in terms of warmth, highlighting the effectiveness of the biological motion profile in conveying warmth in HRI scenarios. The findings that the mean values for the fluidity of motion, naturalness of movement, and perceived friendliness were significantly higher when biological motion was incorporated into the robot's movements have important implications. These results suggest that leveraging biological motion principles can enhance positive user experiences during HRIs. Higher ratings of

fluidity and naturalness indicate that biological motion helped the robot's movements appear more aligned with human motion patterns. This increased sense of familiarity and biomimicry can reduce the perception of robots as mechanical, unfamiliar entities, potentially mitigating feelings of discomfort during interactions.

The higher ratings of perceived friendliness associated with biological motion have significant implications for building positive relationships between humans and social robots. Friendly and approachable demeanors can encourage users to feel more comfortable, engaged, and willing to interact with social robots, potentially increasing acceptance and adoption rates in various application domains.

8.3.2. *Discomfort dimension analysis*

The overall discomfort dimension for the two condition was analyzed following three key attributes: *perceived unnaturalness, awkwardness and unease*, and *perceived uncertainty*. This dimension is reverse-scored, thus a smaller value for discomfort is interpreted as a better interaction experience. Thus, Condition 2 had better results with lesser discomfort values than Condition 1.

The discomfort score for the trapezoidal motion profile was moderate, with a mean of 3.64 (SD = 0.99, SE = 0.24). The analysis showed no significant deviation from the midpoint ($t(16) = -1.49$, $p = 0.156$), with a mean difference of -0.36 and a 95% confidence interval spanning from -0.87 to 0.15. This indicates that the trapezoidal profile did not strongly evoke discomfort but was not significantly lower than the midpoint. The biological motion profile yielded a significantly lower discomfort score, with a mean of 2.59 (SD = 0.86, SE = 0.21). The analysis revealed a significant difference from the midpoint ($t(16) = -6.80$, $p < 0.001$), with a mean difference of -1.41 and a 95% confidence interval ranging from -1.85 to -0.97. These results demonstrate that the biological profile effectively minimized discomfort, falling well below the neutral point. This suggests that biologically inspired gestures contribute to a more positive and less unsettling interaction.

The mean of the aspects of the discomfort dimension under both conditions is shown in Fig. 8. This figure reveals lower ratings of discomfort in biological motion (in shades of green) when compared with the trapezoidal motion profile (in shades of red), demonstrating its ability to evoke a more positive perception of the robot's behavior.

Perceived Unnaturalness: Participants rated the unnaturalness of the gestures lower when performed with the biological motion profile (Condition 2) compared to the linear velocity profile. For the trapezoidal motion profile, the mean score for Perceived Unnaturalness was 4.94 (SD = 1.16, SE = 0.28). The analysis showed a significant deviation from the midpoint ($t(16) = 3.35$, $p = 0.004$), with a mean difference of 0.94 and a 95% confidence interval of 0.35–1.54. These results indicate that the trapezoidal profile was perceived as unnatural. In contrast, the biological motion profile achieved a lower mean score of 2.97 (SD = 1.33, SE = 0.32). The analysis revealed a significant difference from the midpoint ($t(16) = -3.20$, $p = 0.006$), with a
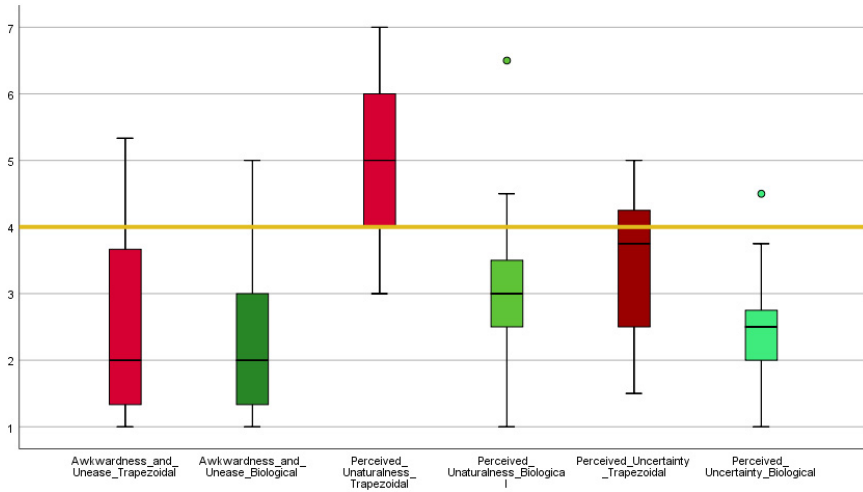
Fig. 8.   Mean of responses of different aspects in the discomfort dimension of both conditions.

mean difference of -1.03 and a 95% confidence interval of -1.71 to -0.35. This suggests that the biological profile was perceived as more natural compared to the neutral midpoint. Both profiles were analyzed relative to the midpoint of the scale. The trapezoidal profile was rated as significantly unnatural, while the biological motion profile was rated as significantly more natural. These results suggest that biologically inspired motion may reduce the perception of unnaturalness in robot movements, as evidenced by the ratings relative to the neutral point. Thus, incorporating a biological motion profile introduces some level of naturalness to the robot's movements.

Awkwardness and Unease: The biological motion profile was perceived as less awkward and causing less unease than the linear velocity profile. The trapezoidal motion profile resulted in a mean score of 5.53 (SD = 1.42, SE = 0.35). The analysis revealed a significant difference from the midpoint $(t(16) = -4.26, p = 0.001)$, with a mean difference of -1.47 and a 95% confidence interval of -2.20 to -0.74. These results indicate that the trapezoidal profile evoked significant discomfort. The biological motion profile achieved a substantially lower mean score of 2.31 (SD = 1.15, SE = 0.28). The analysis showed a significant difference from the midpoint $(t(16) = -6.07, p < 0.001)$, with a mean difference of -1.69 and a 95% confidence interval of -2.28 to -1.10. These findings suggest that the biological profile minimized awkwardness and unease effectively. Both motion profiles demonstrated significant deviations from the neutral midpoint, This could be due to the appealing physical form of the Pepper humanoid robot.[51] These results highlight the potential of biologically inspired motion to enhance the perceived smoothness and comfort of robot gestures.

Perceived Uncertainty: Participants rated the gestures as less uncertain or hesitant when performed with the biological motion profile. The trapezoidal motion profile resulted in a mean score of 3.46 (SD = 1.05, SE = 0.25). The analysis showed a significant difference from the midpoint ($t(16) = -2.14$, $p = 0.049$), with a mean difference of -0.54 and a 95% confidence interval of -1.08 to -0.004. These findings suggest a moderate level of perceived uncertainty with the trapezoidal profile. The biological motion profile yielded a much lower mean score of 2.49 (SD = 0.83, SE = 0.20). The analysis showed a highly significant difference from the midpoint ($t(16) = -7.56$, $p < 0.001$), with a mean difference of -1.51 and a 95% confidence interval of -1.94 to -1.09. These results indicate that the biological profile effectively minimized uncertainty. These results highlight the potential of biologically inspired motion to reduce perceptions of uncertainty in robot gestures, suggesting a smoother and more confident movement style when using the biological motion profile.

Paired *t*-test: In order to understand the actual difference between the discomfort dimensions in the two conditions, a paired *t*-test was conducted between the overall discomfort dimension for the linear and biological motion profiles. The results showed a statistically significant difference ($t = 3.972$, $p = 0.001$), indicating that the linear velocity profile was perceived as significantly causing more discomfort than the biological motion profile.

The lower ratings of perceived unnaturalness of movement associated with biological motion indicate that users found the robot's motions to be more lifelike, biomimetic, and aligned with human kinematic profiles. This decrease in unnaturalness can contribute to a heightened sense of familiarity and social presence, facilitating more seamless and engaging interactions. When users perceive a robot's movements as natural and intuitive, they may be more likely to view the robot as a relatable social entity, fostering stronger anthropomorphic perceptions and emotional connections.

The lower ratings of perceived uncertainty associated with biological motion are also noteworthy. Uncertainty in robotic systems can stem from unpredictable or unfamiliar behaviors, which can hinder trust, understanding, and effective communication. By incorporating biological motion cues, which are deeply ingrained in the human perceptual system,[52] users may have found the robot's actions and intentions more predictable and interpretable, reducing feelings of uncertainty and ambiguity during interactions.

Collectively, these results suggest that adopting biologically inspired motion in social robots can contribute to more natural and potentially more comfortable user experiences. Trajectory analysis of the robot's arm movements, along with joint state measurements, demonstrates that the biological motion profile more closely aligns with human-like kinematic patterns. Such alignment may improve the predictability and familiarity of the robot's gestures, subtly enhancing the robot's approachability and the user's perception of its social qualities.[53] However, these benefits were

observed only in specific aspects, as not all dimensions of user perception showed statistically significant differences between motion profiles. This suggests that while biologically inspired motions offer promising enhancements to robotic behavior, further investigation is needed to understand their impact across diverse social attributes and interaction contexts.

9. Summary and Conclusion

This study explored the integration of biologically inspired motion in gestural communication for social robots, with the objective of enhancing the naturalness, expressiveness, and overall quality of human-robot interactions. The motivation stemmed from the growing need for robots to interact with humans in ways that are intuitive, engaging, and aligned with human expectations. By embedding biological motion principles — specifically, the minimum jerk model — into the gestures of a Pepper humanoid robot, this research aimed to improve perceptions of warmth and reduce discomfort during interactions.

The experimental methodology involved implementing a deictic gesture using two distinct motion profiles: a trapezoidal velocity profile and a biologically inspired motion profile. These gestures were executed with the same time duration across both profiles, ensuring comparability while revealing the smoother transitions characteristic of the biologically inspired motion. The user evaluation involved a structured survey based on the RoSAS, where participants rated the robot's gestures on dimensions of warmth and discomfort. Quantitative trajectory and joint state analyses were also performed, using motion capture with an Intel RealSense camera and ArUco markers, to validate the accuracy and consistency of the robot's motions.

The results demonstrated that gestures executed with the biologically inspired profile were perceived as more natural and fluid, contributing to higher warmth ratings and reduced discomfort in specific dimensions compared to the trapezoidal profile. Statistical analyses revealed significant differences in perceptions for some attributes, while others remained comparable. Motion analysis further confirmed that the biological profile aligns more closely with human kinematics, showing smoother trajectories and fewer abrupt transitions, which are likely to contribute to positive social perceptions.

With a view to widening the breadth of the study described in this paper, we plan on running more in-person studies with a copresent robot, and we are also exploring the possibility of conducting studies online using videos, i.e., using a telepresent robot. Li[54] showed that users perceive copresent robots more positively than telepresent robots, while Donnermann *et al.*[55] found that there are no significant differences between video presentations and physically present robots in user studies of robots acting as tutors. Both approaches have advantages and limitations, e.g., the greater reach of online studies versus the immediacy of in-person studies. Since we are primarily concerned here with the perception of gestures where the robot hands move in three dimensions, and not just in the efficacy of the interaction, it may

be the case that in-person studies with a copresent robot are better suited than 2D videos of a telepresent robot. It would be important to conduct a baseline evaluation of identical studies using both formats before drawing any strong conclusions on their relative merits and committing to a large-scale online study.

In conclusion, this study underscores the potential of biological motion to improve certain aspects of social robot interactions, such as naturalness, fluidity, and perceived warmth. While the findings are promising, further research is needed to explore the broader applicability of these motion models across diverse robot platforms, gesture types, and interaction scenarios.

Acknowledgments

ORCID

Adedayo Akinade ⬤ https://orcid.org/0009-0009-3917-4204
Daniel Barros ⬤ https://orcid.org/0009-0009-0283-8206
David Vernon ⬤ https://orcid.org/0000-0002-9782-3788

References

1. M. Sarrica, S. Brondi and L. Fortunati, How many facets does a "social robot" have? A review of scientific and popular definitions online, *Inf. Technol. People* **33**(1) (2020) 1–21.
2. N. Spatola, S. Marchesi and A. Wykowska, Different models of anthropomorphism across cultures and ontological limits in current frameworks the integrative framework of anthropomorphism, *Front. Robot. AI* **9** (2022) 863319.
3. M. M. A. de Graaf, S. Ben Allouch and J. A. G. M. van Dijk, What makes robots social?: A user's perspective on characteristics for social human-robot interaction, in *Social Robotics*, eds. A. Tapus, E. André, J.-C. Martin, F. Ferland and M. Ammi (Springer International Publishing, Cham, 2015), pp. 184–193.
4. B. Postnikoff and I. Goldberg, Robot social engineering: Attacking human factors with non-human actors, in *Companion of the 2018 ACM/IEEE Int. Conf. Human-Robot Interaction* (Association for Computing Machinery, New York, 2018), pp. 313–314.
5. A. Meghdari, A. Shariati, M. Alemi, G. Vossoughi, A. Eydi, E. Ahmadi, B. Mozafari, A. A. Nobaveh and R. Tahami, Arash: A social robot buddy to support children with cancer in a hospital environment, *Proc. Inst. Mech. Eng. H, J. Eng. Med.* **232**(6) (2018) 605–618.
6. M. M. Neumann, Social robots and young children's early language and literacy learning, *Early Child. Educ. J.* **48** (2019) 157–170.
7. M. A. Kipriyanova and S. Smolnikov, Specialists training in a technical university in the transition to a robotic society, *SHS Web Conf.* **121** (2021) 03005.
8. P. Elsy, Elderly care in the society 5.0 and kaigo rishoku in Japanese hyper-ageing society, *J. Stud. Komun.* **4**(2) (2020) 435–452.

9. S. E. Jung and E.-S. Won, Systematic review of research trends in robotics education for young children, *Sustainability* **10**(4) (2018) 105.

10. K. Dautenhahn, Socially intelligent robots: Dimensions of human–robot interaction, *Philos. Trans. R. Soc. B, Biol. Sci.* **362**(1480) (2007) 679–704.

11. S. M. Fiore, T. J. Wiltshire, E. J. C. Lobato, F. Jentsch, W. Huang and B. Axelrod, Toward understanding social cues and signals in human–robot interaction: Effects of robot gaze and proxemic behavior, *Front. Psychol.* **4** (2013) 859.

12. J. A. Pepito, H. Ito, F. Betriana, T. Tanioka and R. C. Locsin, Intelligent humanoid robots expressing artificial humanlike empathy in nursing situations, *Nurs. Philos.* **21**(4) (2020) e12318.

13. L. Marcinowicz, J. Konstantynowicz and C. Godlewski, Patients' perceptions of GP non-verbal communication: A qualitative study, *Br. J. Gen. Pract.* **60**(571) (2010) 83–87.

14. K. Zougkou, N. Weinstein and S. Paulmann, ERP correlates of motivating voices: Quality of motivation and time-course matters, *Soc. Cogn. Affect. Neurosci.* **12**(10) (2017) 1687–1700.

15. N. Weinstein, M. Vansteenkiste and S. Paulmann, Listen to your mother: Motivating tones of voice predict adolescents' reactions to mothers, *Dev. Psychol.* **55**(12) (2019) 2534–2546.

16. M. S. Mast, J. A. Hall, C. Klöckner and E. M. Choi, Physician gender affects how physician nonverbal behavior is related to patient satisfaction, *Med. Care* **46**(12) (2008) 1212–1218.

17. G. Di Cesare, F. Vannucci, F. Rea, A. Sciutti and G. Sandini, How attitudes generated by humanoid robots shape human brain activity, *Sci. Rep.* **10**(1) (2020) 16928.

18. M. A. Giese and T. Poggio, Neural mechanisms for the recognition of biological movements, *Nat. Rev. Neurosci.* **3**(2) (2003) 179–192.

19. A. Bisio, A. Sciutti, F. Nori, G. Metta, L. Fadiga, G. Sandini and T. Pozzo, Motor contagion during human-human and human-robot interaction, *PLoS One* **9**(8) (2014) e106172.

20. M. Edraki, P. Maurice and D. Sternad, Humans need augmented feedback to physically track non-biological robot movements, in *2023 IEEE Int. Conf. Robotics and Automation (ICRA)* (IEEE, 2023), pp. 9872–9878.

21. A. Puce, A. Rossi and F. J. Parada, Biological motion, in *Brain Mapping*, ed. A. W. Toga (Academic Press, Waltham, 2015), pp. 125–130.

22. P. Viviani and C. Terzuolo, Trajectory determines movement dynamics, *Neuroscience* **7**(2) (1982) 431–437.

23. P. Viviani and G. McCollum, The relation between linear extent and velocity in drawing movements, *Neuroscience* **10**(1) (1983) 211–218.

24. F. Lacquaniti, C. Terzuolo and P. Viviani, The law relating the kinematic and figural aspects of drawing movements, *Acta Psychol.* **54**(1) (1983) 115–130.

25. M. J. E. Richardson and T. Flash, Comparing smooth arm movements with the two-thirds power law and the related segmented-control hypothesis, *J. Neurosci.* **22**(18) (2002) 8201–8211.

26. D. Huh and T. J. Sejnowski, Spectrum of power laws for curved hand movements, *Proc. Natl. Acad. Sci. USA* **112**(29) (2015) E3950–E3958.

27. S. Vieilledent, Y. Kerlirzin, S. Dalbera and A. Berthoz, Relationship between velocity and curvature of a human locomotor trajectory, *Neurosci. Lett.* **305**(1) (2001) 65–69.

28. P. Viviani, G. Baud-Bovy and M. Redolfi, Perceiving and tracking kinesthetic stimuli: Further evidence of motor-perceptual interactions, *J. Exp. Psychol., Hum. Percept. Perform.* **23**(4) (1997) 1232–1252.

29. P. Viviani and N. Stucchi, Biological movements look uniform: Evidence of motor-perceptual interactions, *J. Exp. Psychol., Hum. Percept. Perform.* **18**(3) (1992) 603–623.

30. R. Flach, G. Knoblich and W. Prinz, The two-thirds power law in motion perception, *Vis. Cogn.* **11**(2–3) (2004) 461–481.

31. S. Kandel, J.-P. Orliaguet and P. Viviani, Perceptual anticipation in handwriting: The role of implicit motor competence, *Atten. Percept. Psychophys.* **62**(4) (2012) 706–716.

32. P. Viviani and R. Schneider, A developmental study of the relationship between geometry and kinematics in drawing movements, *J. Exp. Psychol., Hum. Percept. Perform.* **17**(1) (1991) 198–218.

33. P. Viviani and T. Flash, Minimum-jerk, two-thirds power law, and isochrony: Converging approaches to movement planning, *J. Exp. Psychol., Hum. Percept. Perform.* **21**(1) (1995) 32–53.

34. P. Viviani and M. Cenzato, Segmentation and coupling in complex movements, *J. Exp. Psychol., Hum. Percept. Perform.* **11**(6) (1985) 828–845.

35. T. Flash and N. Hogan, The coordination of arm movements: An experimentally confirmed mathematical model, *J. Neurosci.* **5**(7) (1985) 1688–1703.

36. Z. Hasan, Optimized movement trajectories and joint stiffness in unperturbed, inertially loaded movements, *Biol. Cybern.* **53**(6) (1986) 373–382.

37. J. Wann, I. Nimmo-Smith and A. M. Wing, Relation between velocity and curvature in movement: Equivalence and divergence between a power law and a minimum-jerk model, *J. Exp. Psychol., Hum. Percept. Perform.* **14**(4) (1988) 622–637.

38. Y. Uno, M. Kawato and R. Suzuki, Formation and control of optimal trajectory in human multijoint arm movement — Minimum torque-change model, *Biol. Cybern.* **61**(2) (1989) 89–101.

39. H. Nagasaki, Asymmetric velocity and acceleration profiles of human arm movements, *Exp. Brain Res.* **74**(2) (2004) 319–326.

40. N. Hogan and T. Flash, Moving gracefully: Quantitative theories of motor coordination, *Trends Neurosci.* **10**(4) (1987) 170–174.

41. W. P. Chan, T. Tran, S. Sheikholeslami and E. Croft, An experimental validation and comparison of reaching motion models for unconstrained handovers: Towards generating humanlike motions for human-robot handovers, in *Proc. 20th IEEE-RAS Int. Conf. Humanoid Robots (HUMANOIDS 2020)* (IEEE, United States of America, 2021), pp. 356–361.

42. M. Huber, H. Radrich, C. Wendt, M. Rickert, A. Knoll, T. Brandt and S. Glasauer, Evaluation of a novel biologically inspired trajectory generator in human-robot interaction, in *RO-MAN 2009 — 18th IEEE Int. Symp. Robot and Human Interactive Communication* (IEEE, 2009), pp. 639–644.

43. N. Hogan, An organizing principle for a class of voluntary movements, *J. Neurosci.* **4**(11) (1984) 2745–2754.

44. D. Vernon, System architecture, CSSR4Africa Deliverable D3.1 (2024), https://cssr4africa.github.io/deliverables/CSSR4Africa_Deliverable_D3.1.pdf.

45. C. M. Carpinella, A. B. Wyman, M. A. Perez and S. J. Stroessner, The robotic social attributes scale (RoSAS): Development and validation, in *Proc. 2017 ACM/IEEE Int. Conf. Human-Robot Interaction, HRI '17* (Association for Computing Machinery, New York, 2017), pp. 254–262.

46. N. Spatola and O. A. Wudarczyk, Implicit attitudes towards robots predict explicit attitudes, semantic distance between robots and humans, anthropomorphism, and prosocial behavior: From attitudes to human-robot interaction, *Int. J. Soc. Robot.* **13** (2021) 1149–1159.

47. S. Mandl, M. Bretschneider, S. Meyer, D. Gesmann-Nuissl, F. Asbrock, B. Meyer and A. Strobel, Embodied digital technologies: First insights in the social and legal perception of robots and users of prostheses, *Front. Robot. AI* **9** (2022) 787970.

48. J. Jørgensen and M. B. Christiansen, The sounds of softness. Designing sound for human-soft robot interaction, *Front. Robot. AI* **8** (2021) 674121.

49. B. Scassellati, H. Admoni and M. J. Matarić, Robots for use in autism research, *Annu. Rev. Biomed. Eng.* **14** (2012) 275–294.

50. R. Oliveira, P. Arriaga, S. J. Stroessner and A. Paiva, Preliminary validation of the european portuguese version of the robotic social attributes scale (RoSAS), *Hum. Behav. Emerg. Technol.* **3**(5) (2021) 750–758.

51. D. Vernon and G. Sandini, The importance of being humanoid, *Int. J. Humanoid Robot.* **21**(1) (2024) 2350022.

52. F. Simion, L. Regolin and H. Bulf, A predisposition for biological motion in the newborn baby, *Proc. Natl. Acad. Sci. USA* **105**(2) (2008) 809–813.

53. A. Vignolo, N. Noceti, F. Rea, A. Sciutti, F. Odone and G. Sandini, Detecting biological motion for human–robot interaction: A link between perception and action, *Front. Robot. AI* **4** (2017) 14.

54. J. Li, The benefit of being physically present: A survey of experimental works comparing copresent robots, telepresent robots and virtual agents, *Int. J. Hum.-Comput. Stud.* **77** (2015) 23–37.

55. M. Donnermann, P. Heinzmann and B. Lugrin, Meet or call my robotic tutor? — The effect of a physically vs. virtually present social robot on learning outcomes, engagement and perception, in *HRI '24: Companion of the 2024 ACM/IEEE Int. Conf. Human-Robot Interaction* (Association for Computing Machinery, New York, 2024), pp. 422–426.

Adedayo Akinade received his Bachelor of Engineering from the Federal University of Agriculture, Nigeria, in 2021, and his Master of Science in Electrical and Computer Engineering, Advanced Studies Program, from the Carnegie Mellon University Africa, in 2024. He works as a Research Associate on a project Culturally Sensitive Social Robotics for Africa, funded by the Mastercard Foundation through the Afretec Network and the Center for the Inclusive Digital Transformation of Africa at CMU-Africa, where he is responsible for the development of overt attention and gestural communication.

Daniel Barros received his Bachelor of Science degree in Electrical Engineering and Information Technology from the Technical University of Munich in 2024. He wrote his Bachelor Thesis on imitation learning and computer vision with the Interactive Skill Learning group at the Robotics and Mechatronics Institute of the German Aerospace Center DLR. He continues his work on learning from demonstration as a research intern at the Carnegie Mellon University Africa on the project Culturally Sensitive Social Robotics for Africa, funded by the Mastercard Foundation through the Afretec Network and the Center for the Inclusive Digital Transformation of Africa.

David Vernon is a Research Professor at the Carnegie Mellon University Africa. He received his B.A. and B.A.I. degrees from the University of Dublin, Trinity College, in 1979, and his Ph.D. degree in 1985. Since graduating, he has held positions at Westinghouse Electric, Trinity College Dublin, the European Commission, National University of Ireland, Maynooth, Science Foundation Ireland, Khalifa University, University of Genoa, Technical University of Munich, University of Skövde, and University of Bremen.

His work focuses on cognitive robotics, with particular emphasis on cognitive architectures. He is the author of over 140 technical publications and four books. He was the technical coordinator of the EU-funded RobotCub project that developed the iCub cognitive humanoid robot. He was a founding co-chair of the IEEE Robotics and Automation Society (RAS) Technical Committee for Cognitive Robotics. He is a Life Senior Member of the IEEE, a Chartered Engineer and Fellow of the Institution of Engineers of Ireland, a Research Fellow at the Kigali Collaborative Research Centre, Rwanda, and a past Fellow of Trinity College Dublin, Ireland.